ACES Asian Chemical Editorial Society

DOI: 10.1002/cnma.202000029

CHEMNANOMAT
Full Paper

Highly Aligned Carbon Nanotube-Based Bi-Material Microactuators with Reduced Intertube Slipping

Peng Zhang,[a, b] Jian Guo,[a, b] Huwang Hou,[a, b] Yiyuan Zhang,[a, b] Xiaochen Yang,[a, b] Hongmei Zhong,[a, b] Lie Chen,[a, b] and Yang Zhao*[a, b]

Abstract: Bi-material microcantilevers have been widely used as both thermal sensors and thermal actuators. Carbon nanotubes (CNT) are prominent candidates for bi-material actuators due to the negative coefficient of thermal expansion (CTE) at the axial direction that allows for higher thermal sensitivity. However, CNT-based actuators generally suffer not only from intertube slipping due to weak interactions between the assembled CNTs but also from poor control over orientation assembly. To address these challenges, a new class of closely packed, highly aligned CNT microcantilevers reinforced by ceramic interlocking is here proposed, followed with deposition of Al thin film to form the bi-material actuators. The investigations of the mechanical properties and thermal response of CNT microcantilevers indicate that the slipping between the tubes limits both the strength and the thermal sensitivity of the bi-material microcantilevers. Intertube deposition of Al_2O_3 as ceramic interlocking is used to reinforce the binding strength between the tubes, and increases in the mechanical strength as well as thermal sensitivity of the microcantilevers have been achieved.

1. Introduction

Microactuators, which can perform certain mechanical motions via external stimuli, are vital to the development of biomimetic robots, artificial muscles, and micromanipulators.[1–5] Thermal microactuators based on bi-materials are widely used in Micro-Electro-Mechanical System (MEMS), stimulated by several sources including visible light or infrared (IR), thermal radiation, or Joule heating. Significant displacement, fast response, and high-energy conversion efficiency are much desired among these applications in recent years. Among the major materials for thermal microactuators including polymers, silicon dioxide, vanadium dioxide and carbon nanotubes (CNT), carbon nanotubes are ideal candidates due to the distinctive negative coefficient of thermal expansion (CTE), which is $-11\times10^{-6}\,K^{-1}$ in the axial direction around room temperature.[6] In a case where a thin layer of CNT film coupled to a positive CTE material is heated, the large mismatch in CTE may lead to large bimorph actuation. Therefore, such design can ensure high temperature sensitivity of the devices. For photothermal actuators specifically, it is essential to have strong optical absorbance to achieve high-energy conversion efficiency.[7] It has been shown that CNTs possess a nearly constant and near-unity emissivity (absorptivity) of 0.98–0.99 across a wide spectral range from UV (200 nm) to far infrared (200 μm),[8] which makes them perfect for energy absorption/converstion material. Furthermore, the thermal time constant of a thermal actuator is determined by the mass density and specific heat of the materials. The mass density of CNT is much smaller than that of other major materials, which can ensure rapid response.

However, inter-tube slipping is one of the most common obstacles lying in CNT fibers, CNT ropes and CNT films. This obstacle degrades the mechanical properties of CNT based materials and limits their potential applications in micro-electro-mechanical systems (MEMS).[9] CNT films or CNT ropes are assembled by individual CNTs through weak van der Walls interaction, which is the root of weak interfacial shear strength between individual CNTs. With stimulation applied to the CNT-based actuators, relative slipping between individual CNTs occurs, causing insufficient load transfer between adjacent nanotubes and reducing the deformation. Hence, inter-tube slipping needs to be addressed before carbon naotubes can deliver high performence actuators.

Previously published studies have developed some methods on the reinforcement of CNT fibers. The most common approaches are irradiation methods and polymer interlocking methods. The structure of CNTs can be modified using electron or ion-beam irradiation by transmission electron microscope (TEM) or focused ion beam (FIB).[10,11] Irradiation methods can introduce stable crosslinks forming with the participation of interstitial carbon atoms or by a radiation-induced chemical reaction between carboxyl groups attached to neighboring nanotubes. However, it is tough to manufacture at a large scale due to the high energy density requirement. Furthermore, irradiation with high energy particles is associated with introducing unwanted defects that further degrade the mechanical performance of the CNT fibers.[12] Polymer interlocking methods take an effective post-treatment approach to introduce polymer chains between CNTs by using aryl radical coupling reaction or in situ chemical vapor deposition.[13,14] The

[a] P. Zhang, J. Guo, H. Hou, Y. Zhang, X. Yang, H. Zhong, Dr. L. Chen, Prof. Dr. Y. Zhao
CAS Key Laboratory of Mechanical Behavior and Design of Materials
University of Science and Technology of China
Hefei, Anhui 230027 (P. R. China)

[b] P. Zhang, J. Guo, H. Hou, Y. Zhang, X. Yang, H. Zhong, Dr. L. Chen, Prof. Dr. Y. Zhao
Department of Precision Machinery and Precision Instrumentation
University of Science and Technology of China
Hefei, Anhui 230027 (P. R. China)
E-mail: yangz1@ustc.edu.cn

enhanced interactions between the bundles were mostly due to non-covalent interactions between the polymer chains introduced onto the surface of the bundles. But the lower intrinsic strength of polymer ultimately limits the overall mechanical properties of CNT fibers.

Herein, we present the development of bi-material micro-cantilevers made of CNT film coupled with Al thin film. In order to utilize the axial properties of CNTs, we fabricated closely packed, highly aligned CNT films. The CNT microcantilevers are defined with Focus Ion Beam (FIB) milling along the alignment direction, followed with deposition of Al thin film to form the bi-material sensors. The investigations of the mechanical properties and thermal response of the microcantilevers indicate that the slipping between the tubes due to weak van der Waals interaction limits not only the strength, but also the thermal sensitivity of the bi-material microcantilevers. Ceramics are commonly used for coating materials because of the good strength to weight ratios, high melting and oxidation temperatures and excellent wear resistance. The porous nature of the CNT films allows researchers to use methods such as atomic layer deposition (ALD) to uniformly inter-tubes deposit Al_2O_3 thin film as reinforcement coating. So we have introduced ceramic interlocking between neighboring carbon nanotubes within films by using ALD, which could simply and effectively limit the slipping between the nanotubes. With the introduction of ceramic interlocking, increases in both the mechanical strength and thermal response of the microcantilevers have been achieved.

2. Results and Discussion

2.1. Preparation of self-supporting CNT film and FIB directly-patterning

Figure 1 shows the schematics of the fabrication process for directly patterned oriented carbon nanotubes cantilevers. First, lines of catalyst for regular arrays on a silicon substrate were patterned through conventional lithography. The catalyst consists of 2 nm thin film of iron with 10 nm thin film of alumina underneath as buffer layer. Second, vertically aligned carbon nanotube (VACNT) sheets almost 2 mm in height (Figure 1(b)) were prepared by the water-assisted chemical vapor deposition (CVD) from the patterned catalyst lines at 760 °C for 40 min, with ethylene as the carbon source and water as the growth enhancer.[15,16] The width of the catalyst line determines the thickness of the VACNT sheets. The volume fraction of VACNT sheets is only 1%, so it is very sparse. Nonetheless, the VACNT sheets could be manipulated as cohesive units due to van der Walls interactions and entanglement between tubes. Then the sparse VACNT sheet was removed from the growth substrate as a freestanding film with tweezers and laid down on another silicon substrate patterned with micropillar arrays. Subsequently, a droplet of isopropyl alcohol (IPA) solution was dispensed on it. The IPA solution is applied to generate a capillary force to reduce the distance among the CNTs as well as between the CNTs and the substrate, thereby producing stronger van der Walls interactions. During the dried process, the capillary force of the liquids drew the fibrous CNT sheet together so that transformed it into closely packed, highly aligned CNT film.[17] The CNT film could

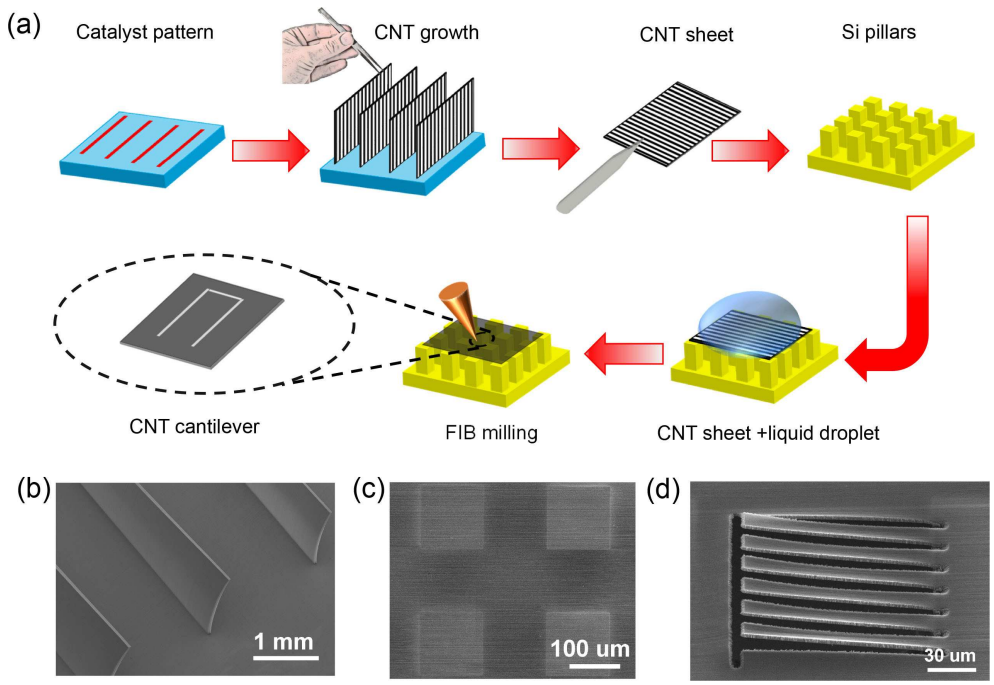

Figure 1. a) Schematic illustration of the fabrication process of the CNT cantilever. SEM images of b) VACNT sheets, c) closely packed, highly aligned CNT film, and d) CNT microcantilevers.

be treated as a single robust body. At the same time, the capillary effect also acted as a preload which brought the CNT film into tight contact with silicon substrate. The adhesion of CNT film to substrate stems also from the van der Walls interactions between the two surfaces.[18] The concentration of the IPA solution was 50% in volume fraction and is critical to achieve effective film densification and sufficient adhesion between the film and substrate. Therefore, the self-supporting densified CNT film, a super-aligned anisotropic material, was successfully prepared. Finally, several CNT microcantilevers paralleled to CNT alignment direction were directly patterned by focused ion beam (FIB) (Figure 1(d)), a powerful direct-writing technique, which is often chosen for micro and nano-fabrication without lithography. These suspended cantilevers could serve as key elements for the study of mechanical properties and actuated performence of the CNT film.

2.2. Mechanical properties measurement

As shown in Figure 2(a), the spring constant K of CNT micro-cantilevers were measured by atomic force microscopy (AFM) (Bruker, Demension Icon) operating in peakforce tapping mode which is a special mode in particular for measuring force curves. The effective Young's modulus of the CNT microcantilever is given by

$$E_{eff} = \frac{4KL^3}{wt^3} \quad (1)$$

where E_{eff} is the effective Young's modulus, K the spring constant, and L, w, t are the length, width, and the thickness of the CNT microcantilevers, respectively. The dimensions of the microcantilevers defined by FIB milling are 120 μm long and 20 μm wide. However, it was too difficult to apply the AFM cantilever tip to the free end of the CNT microcantilevers so that there was a certain distance from the free end. Hence the actual bending length of the CNT microcantilevers is about 100 μm. The thickness was measured to be in a range from 2.1 to 2.2 μm by SEM.

Ceramics are commonly used as conformal coating for vertically aligned CNT arrays to improve compressive strength and stiffness.[19,20] The porous nature of the densified CNT films also allows researchers to use methods such as atomic layer deposition (ALD) to weld the nanostructures of CNTs by uniform inter-tubes deposition of Al_2O_3 thin films.[21] In this study we report on a detailed TEM investigation of these nanostructures in the CNT films. The TEM samples were prepared by ultrasonic treatment of CNT films in beakers filled with ethanol for 15 minutes, followed by dipping copper meshes. As can be seen from Figure 3(a), individual tubes in the CNT films entangle with each other resulting in the formation of branch gaps and nano-junctions denoted as Van der Waals bonds. The Al_2O_3 deposited by ALD can fill the branch gaps between tubes and wrap the nano-junctions as can be seen in Figure 3(d). The nano-junctions are wrapped by a thin layer of Al_2O_3 as ceramic interlock bonds, which are made by drawing the liquid precursor into the porous CNT film and pyrolyzing the precursor. The schematic model of Van der Waals bonded CNT bundles and ceramic interlock bonded CNT bundles are

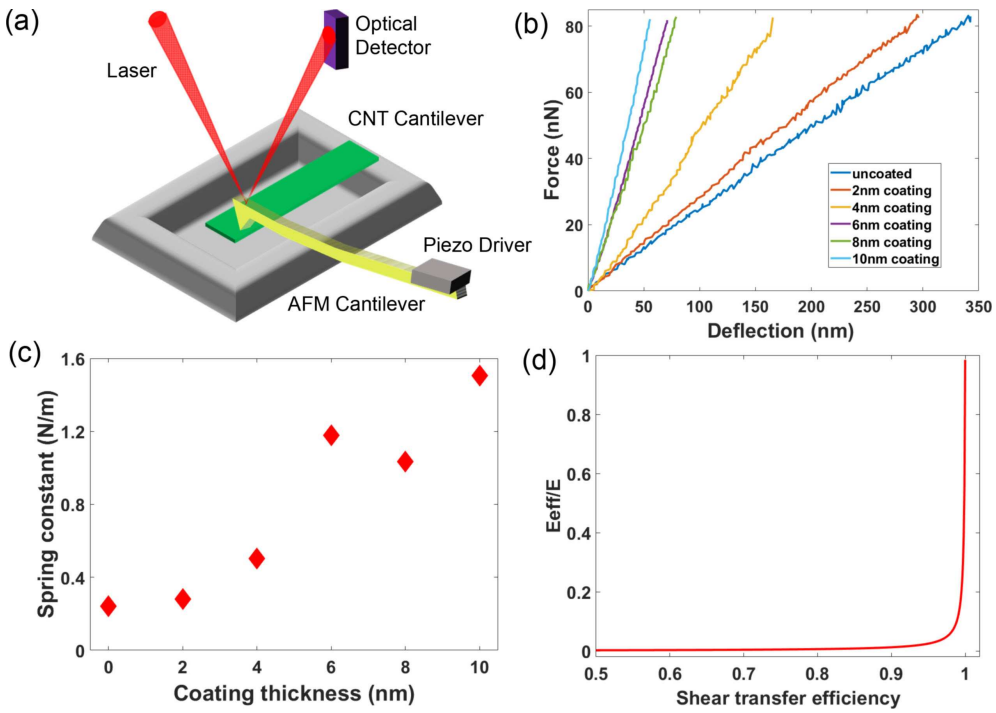

Figure 2. a) Principle of AFM characterization of CNT microcantilever. b) Force curves and c) spring constant of CNT microcantilevers with different coating thickness. d) E_{eff}/E as a function of the shear transfer efficiency.

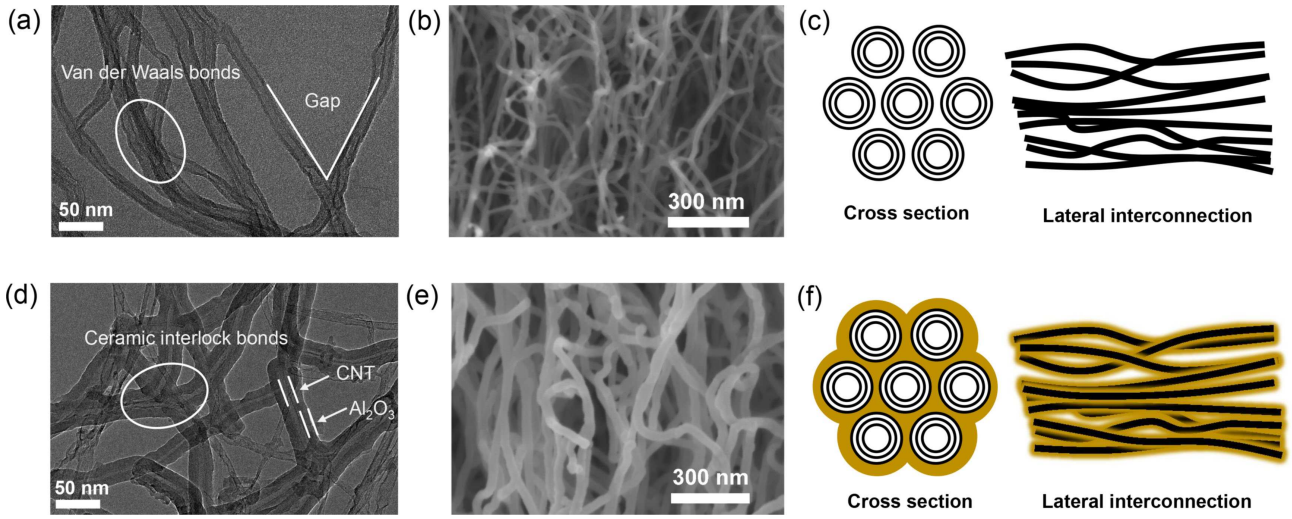

Figure 3. High resolution TEM images of a) Van der Waals bonded CNT bundles and d) ceramic interlock bonded CNT bundles. Schematic model of c) Van der Waals bonded CNT bundles and f) ceramic interlock bonded CNT bundles. Lateral view SEM images of b) Van der Waals bonded CNT film and e) ceramic interlock bonded CNT film.

shown in Figure 3(c) and Figure 3(f). Furthermore, the lateral view SEM images of Van der Waals bonded CNT film and ceramic interlock bonded CNT film are shown in Figure 3(b) and Figure 3(e). A range of alumina thicknesses was tested to investigate the effect of coating thickness to the mechanical behaviors of CNT films. One interesting finding is that the spring constant of the CNT microcantilevers with various coating thickness (0, 2, 4, 6, 8, 10 nm) is varied from 0.24 to 1.5 N/m, as shown in Figure 2(c). Obviously, the uncoated CNT microcantilever exhibited the lowest effective Young's modulus because of the weak interactions between the CNTs which are bound together by entanglements and van der Waals interactions. Figure 2(c) also reveals that a significant improvement of the effective Young's modulus is obtained with the increasing coating thickness. The effective Young's modulus of an uncoated CNT microcantilever has been greatly improved from 6.3 GPa to 40 GPa after reinforcement by 10 nm Al_2O_3 coating. It should be noted that the force-deflection curve of the uncoated CNT microcantilever reveals a characteristic sawtooth-like pattern. The results show that there is a gradual decline in the number of the sawtooth-like pattern with the increase in coating thickness and the pattern became barely visible for 10 nm coated cantilever (Figure 2(b)). It is believed that inter-tube slipping results in the sawtooth-like pattern, and every peak corresponds to the breakage of several nano-junctions, causing the slipping to release stress. This process is similar to the mechanisms of natural coil molecules, such as shells, titin and bones.[22,23] The inter-tube binding energy and the contact length are identified as the two factors that contribute to load transfer in CNT bundles.[24] As the coating thickness increased, an increasing number of branch gaps are filled so that the length of ceramic interlock bonds gradually enlarged. The load is transferred to whole film through shared bonds of adjacent crosslink parts. Consequently, the number of CNTs undergoing shear stress transfer is in continual growth. More importantly, the bonding strength of the nano junctions is greatly enhanced, because the Van der Waals junctions are replaced by the ceramic junctions with stronger binding energy. Therefore, the slipping can be surpressed steadily and the amount of sawtooth-like pattern is significantly declined.

R. Byron Pipes et al. developed a model wherein the shearing traction upon flexural compliance of the CNT array was quantified.[25,26] In this model, the CNT fibers are treated as laminated beams composed of many rectangular layers with the same bending properties at each layer. Assuming that the thickness of individual layers of the laminate is the center distance of two layers of carbon nanotubes. Due to imperfectly bonded between layers, a parameter, $0 \leq k \leq 1$, "shear transfer efficiency" is defined as the ratio of the magnitude of the shearing traction. By introducing imperfect bonding of CNT cantilevers, the shear traction can be continuously varied to evaluate the flexural behavior of CNT cantilevers with varying levels of interfacial shear stress transfer and thereby mimic the interlocking interaction among the CNTs. The fully bonded condition corresponds to $k=1$ where the traditional Euler-Bernoulli beam theory is applicable while the unbonded condition corresponds to $k=0$. When this model is used to describe the mechanical properties of a CNT cantilever, the relationship between the effective Young's modulus of the cantilever and the Young's modulus of an individual multi-walled carbon nanotube can be written as

$$E_{eff} = \frac{\sum_{j=1}^{n} I_j}{I_T - k\left(I_T - \sum_{j=1}^{n} I_j\right)} E \tag{2}$$

where E_{eff} is the effective Young's modulus of the CNT cantilever, E the Young's modulus of an individual multiwalled

carbon nanotube (MWCNT), I_T the total moment of inertia with fully bonded condition, I_j the moment of inertia of an individual layer and n is the total number of layers. The diameter of carbon nanotubes is about 15 nm and the volume fraction of CNT film is 20% in this work. So the equivalent thickness of the individual layer is 75 nm and the total number of layers is 28. Previous study has obtained the value of the Young's modulus of MWCNT, which turned out to be 0.9 TPa from TEM images.[27] The E_{eff}/E is a very strong function of the shear transfer efficiency k, and this relationship is shown in Figure 2(d). What can be clearly seen in this figure is the great improvement of the effective Young's modulus within the range of $k=0.9\sim1$. When substituting the experimental results of AFM measurement into equation (2), the obtained values of k range from 0.819 to 0.973 with various coating thickness. In summary, all these results demonstrate that the formation of ceramic interlocking bonds can effectively suppress the slipping of the CNT films.

2.3. Thermal sensitivity measurement

The thermal sensitivity of a bi-material microcantilever refers to the tip displacement change δ due to the temperature change ΔT.[28] In order to study the effect of ceramic interlocking on thermal sensitivity of CNT based bi-material microcantilevers, we prepared two types of CNT microcantilevers ($L=80$ μm, $w=16$ μm, $t=0.7$ μm), one with 10 nm Al_2O_3 coating and the other without coating, followed with deposition of 20 nm chromium and 200 nm aluminum by sputtering to form the bi-material actuators. The thin chromium layer serves as adhesion promoter between the CNT films and aluminum layer. When the temperature changes by ΔT, the two layers bounded to each other exhibit different thermal strains, which then generate thermal stresses at the interface, thus bending the microcantilevers. The samples, which contain bi-material microcantilevers, were characterized by the experimental setup shown in Figure 4(a). Figure 4(b) and Figure 4(c) present the profiles of one of bi-material microcantilvers before and after thermal loading. The initial shape of the bi-material microcantilever was upwarped because of intrinsic stress, and it bended downward after the thermal loading. In this way, the temperature sensitivity of the actuators can be characterized.

The relationship of the deflection $z(x)$ at a location x and temperature rise for a bi-material microcantilever can be found by solving the thermomechanical governing equation,[29–31]

$$\frac{d^2z}{dx^2} = 6(\alpha_{Al} - \alpha_{CNT})\left(\frac{t_{Al}+t_{CNT}}{t_{CNT}^2 K}\right)\Delta T \tag{3}$$

Where

$$K = 4 + 6n + 4n2 + \phi n3 + \frac{1}{\phi n} \tag{4}$$

Here α is the thermal expansion coefficient, t the thickness of each layer, ΔT the temperature rise of the microcantilever, $n=t_{Al}/t_{CNT}$ the thickness radio, and $\phi=E_{Al}/E_{CNT}$ is the elastic modulus ratio. It is assumed that the temperature is uniform in any cross section of the microcantilever, this is reasonable since the microcantilever is very thin compared to its length. The thermal sensitivity can be obtained from equation (3) and written as

$$S = \frac{\delta}{\Delta T} = 3(\alpha_{Al} - \alpha_{CNT})\left(\frac{n+1}{K}\right)\left(\frac{L^2}{d_{CNT}}\right) \tag{5}$$

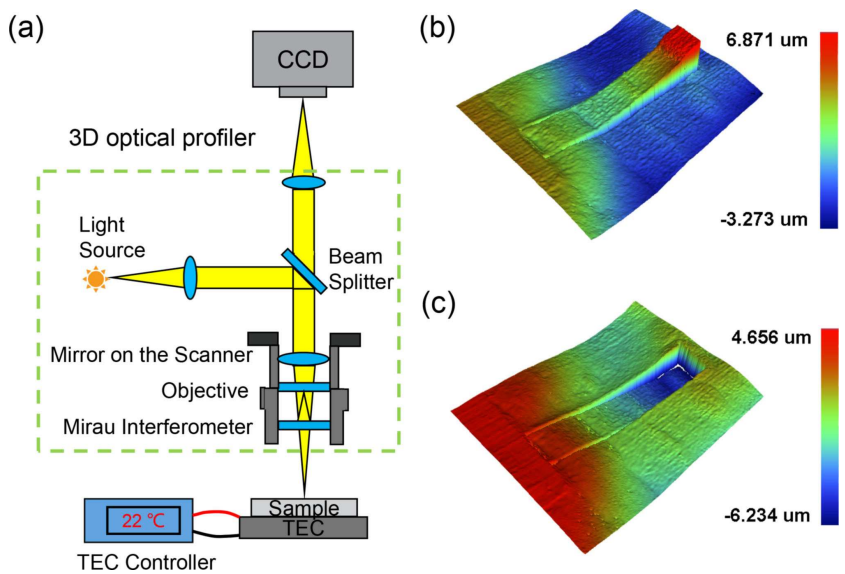

Figure 4. a) Schematic of thermal response test setup including thermal loading stage and optical profiler. The profile of a sample b) before and c) after thermal loading.

in which L is the length of the microcantilever and δ is the tip deflection. It is clear that S strongly depends on the thickness ratio n of the two materials. Equation (4) shows that when $n \to 0$ or $n \to \infty$, the factor $K \to \infty$ and, hence, $S \to 0$. This physically means that in the limit when one of the layers is much thinner than the other, the thermal sensitivity goes to zero.

The deformation profiles of one of the 80×16 μm Al-CNT bi-material microcantilevers along the length direction are shown in Figure 5(a) (10 nm alumina coating) and Figure 5(b) (uncoated), respectively. Each figure contains six sets of data point corresponding to deflection profiles at different temperature, which changed from 22 °C to 72 °C with an interval of 10 °C. Surprisingly, the thermomechanical deformation of bi-material microcantilevers with 10 nm alumina coating was observed to be significantly larger than uncoated microcantilevers even though the effective Young's modulus of the coated one is much higher than that of the uncoated one. In order to quantify the difference between the two thermomechanical deformation, the tip displacement of the microcantilevers at different temperature is plotted and fitted in Figure 5(c) to calculate the thermal sensitivity that is represented by the slopes of the fitting lines. The fitting results show that the thermal sensitivity of CNT based bi-material microcantilevers with and without ceramic interlocking is 0.125 μm/K and 0.079 μm/K correspondently. Therefore, the thermal sensitivity of CNT based actuators can be significantly improved when the slipping between the CNTs is effectively suppressed.

The above results show that CNT arrays directly assembled into films cannot be efficiently used as thermal microactuators because of dominant slipping between tubes. The ceramic interlock bonding of CNTs provides a significant reduction of slipping and increase the thermal sensitivity of the CNT-based thermal actuators. According to the above, the thermomechanical response is closely related to thickness ratio of the two materials. The size and thickness configuration of the two measured samples are the same, except that the CNT layer of one of them forms ceramic interlock bonding and the other one does not. However, our experiment results indicate that the actual thermomechanical response of ceramic interlock bonded bi-material microcantilever is much larger than bare CNT based bi-material microcantilever. The reasonable explanation for this phenomenon is that the slipping between the tubes in bare CNT film makes the CNT layer that actually undergoes the thermal deformation is much thinner than the metal layer (Figure 5(d)), resulting in a low sensitivity. Therefore, if the slipping between tubes is limited, the potential application of CNT films or fibers in microactuators can be exploited to a greater extent.

3. Conclusion

In conclusion, we have successfully fabricated a kind of closely packed, highly aligned CNT films, whose properties in the axial direction can be easily taken advantage of. The microcantilevers were defined with FIB milling on the self-supporting CNT films, followed with deposition of Al thin film to form the CNT-based bi-material microactuators. The mechanical properties of bare

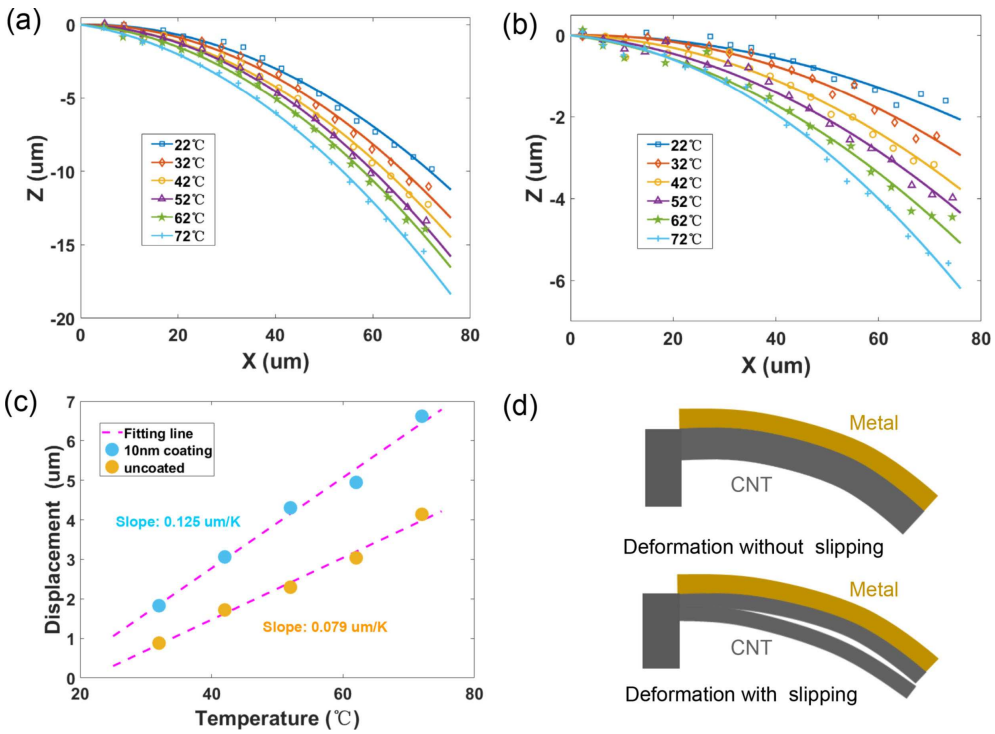

Figure 5. Height profiles of a) uncoated and b) 10 nm coating thickness bi-material microcantilevers. c) Tip displacement of the microcantilevers as a function of temperature. d) Schematic diagram of bi-material microcantilevers with and without slipping.

and ceramic interlock-bonded CNT microcantilevers with different ceramic coating thickness were investigated through AFM. It was observed that ceramic interlockbonded CNT microcantilevers exhibited significant improvement in Young's modulus, reduction in the sawtooth-like pattern of the mechanical curves and enhancement in shear transfer efficiency, which indicated that the introduction of ceramic interlock could effectively eliminate the slipping between CNTs. Subsequently, we have used a combination of an optical measurement apparatus based on white light interference and a heating stage with closed-loop control to characterize the thermomechanical bending of the bi-material microcantilevers. As a result, the achieved bi-material microactuators based on ceramic interlockbonded CNT film are less affected by intertube slipping and exhibit higher thermal sensitivity than those based on bare CNT film. In the longer term, this work could open new routes toward the development and improvement of novel microrobotics, biomedical applications and artificial muscles.

Experimental Section

Growth of VACNT sheets: Vertically aligned carbon nanotube (VACNT) sheets almost 2 mm in height (Figure 1(b)) were prepared by the water-assisted chemical vapor deposition (CVD) from the catalyst lines patterned using lithography (SUSS MABA6) on a silicon substrate at 760°C for 40 min. The patterning process of catalysts was as follows: First, a 10-nm buffer layer of alumina and a 2-nm layer of iron as catalysts were subsequently deposited onto the Si substrate by ALD (Picosun, Sunale R-200 Advanced) and thermal evaporation (VNANO, Beijing, China, VZZ-300). Second, 1-μm-thick photoresist (AZ 5214) was exposed and developed, and then the thin film of catalyst was etched by inductively coupled plasma (ICP) (Oxford, Plasma Pro System 100 ICP 180). Finally, acetone was used to remove the residual photoresist. The growth of VACNT sheets was done in argon (Ar) and hydrogen (H_2) with ethylene (C_2H_4) as the carbon source and water as the growth enhancer in a tube furnace (KEJING, Hefei, China, OTF-1200X). First, the prepared substrate with patterned catalysts was put into the reaction tube and a flow of Ar (126 sccm) was also introduced into the tube later. A current of H_2 (80 sccm) flowed into the tube when the temperature of the furnace rose to 550 °C. Once the furnace reached the target temperature 760 °C, a mixture of C_2H_4 with a flow rate of 54 sccm and a small amount of water vapor (~ 125 ppm) was supplied into the reaction tube to start the growth stage. The growth stage took about 40 min then the sample was cooled down to room temperature in Ar.

Fabrication of CNT microcantilevers: The ion source of FIB is usually liquid metal gallium or helium. In this work, a focused ion beam system (FEI Helios 650) with source of liquid metal gallium was used for pre-designed microcantilevers outline milling. The acceleration voltage of Ga+ was 30 kV and the ion current was 65 nA. The CNT film was partially translucent under the scanning electron microscope (Figure 1(c)), so the suspended part of the film and locations of the micropillars underneath the film can be easily identified.

Experimental setup of thermal sensitivity measurement: The samples, which contain bi-material microcantilevers, were characterized by the experimental setup shown in Figure 4(a). The samples were heated by a thermoelectric cooler (TEC) which was controlled by a TEC controller to maintain deviations in the temperature within 0.01 °C. The temperature at the surface of the silicon substrate was monitored using a thermal couple for closed-loop temperature control. In order to attain thermal equilibrium, the samples were kept at a constant temperature for about 2 min before measurement. Each tested microcantilever was subjected to five stages of thermal loading from 22 °C to 72 °C. The deflection profiles of the microcantilevers were recorded by a 3D optical profiler (Bruker GT–K), which uses the white light interferometry technique to measure and image three-dimensional surfaces.

Characterization: Transmission electron microscopy (TEM) and scanning electron microscopy (SEM) images were recorded on Hitachi SU8220 (Hitachi) and JEM-2100F (JEOL), respectively. The mechanical properties of CNT microcantilevers were measured by atomic force microscopy (AFM) (Bruker, Demension Icon) operating in peakforce tapping mode.

Acknowledgements

This work was supported by the National Natural Science Foundation of China (#11772321 and #51732006) and the Chinese 1000 Young Talented Program. We would like to thank the USTC Center for Micro and Nanoscale Research and Fabrication for the support in the microfabrication process.

Keywords: carbon nanotubes · bi-material microcantilevers · thermal actuator · ceramic interlock bond · reduced slipping

[1] H. Conley, N. V. Lavrik, D. Prasai, K. I. Bolotin, *Nano Lett.* **2011**, 11, 4748.
[2] B. Han, Y. L. Zhang, L. Zhu, Y. Li, Z. C. Ma, Y. Q. Liu, X. L. Zhang, X. W. Cao, Q. D. Chen, C. W. Qiu, H. B. Sun, *Adv. Mater.* **2019**, *31*, e1806386.
[3] K. Liu, C. Cheng, Z. Cheng, K. Wang, R. Ramesh, J. Wu, *Nano Lett.* **2012**, *12*, 6302.
[4] H. Ma, J. Hou, X. Wang, J. Zhang, Z. Yuan, L. Xiao, Y. Wei, S. Fan, K. Jiang, K. Liu, *Nano Lett.* **2017**, *17*, 421.
[5] S. E. Zhu, R. Shabani, J. Rho, Y. Kim, B. H. Hong, J. H. Ahn, H. J. Cho, *Nano Lett.* **2011**, *11*, 977.
[6] Y. K. Kwon, S. Berber, D. Tomanek, *Phys. Rev. Lett.* **2004**, *92*, 015901.
[7] Y. Zhang, J. Ma, S. Liu, D. Han, Y. Liu, Z. Chen, J. Mao, H. Sun, *Nano Energy* **2020**, *68*, 104302.
[8] K. Mizuno, J. Ishii, H. Kishida, Y. Hayamizu, S. Yasuda, D. N. Futaba, K. Hata, *Proc. Natl Acad. Sci* **2009**, *106*, 6044.
[9] A.-S. Michardière, C. Mateo-Mateo, A. Derré, M. A. Correa-Duarte, N. Mano, P. Poulin, *J. Phys. Chem. C* **2016**, *120*, 6851.
[10] T. Filleter, R. Bernal, S. Li, H. D. Espinosa, *Adv. Mater.* **2011**, *23*, 2855.
[11] A. Kis, G. Csanyi, J. P. Salvetat, T. N. Lee, E. Couteau, A. J. Kulik, W. Benoit, J. Brugger, L. Forro, *Nat. Mater.* **2004**, *3*, 153.
[12] Z. Xu, L. Xu, F. Fang, H. Gao, W. Li, *Nuclear Instruments and Methods in Physics Research Section B: Beam Interactions with Materials and Atoms* **2013**, *307*, 203.
[13] M. Naraghi, G. H. Bratzel, T. Filleter, Z. An, X. Wei, S. T. Nguyen, M. J. Buehler, H. D. Espinosa, *Adv. Funct. Mater.* **2013**, *23*, 1883.
[14] O.-K. Park, W. Lee, J. Y. Hwang, N.-H. You, Y. Jeong, S. M. Kim, B.-C. Ku, *Composites Part A: Applied Science and Manufacturing* **2016**, *91*, 222.
[15] L. Chen, B. Ju, Z. Feng, Y. Zhao, *Smart Mater. Struct.* **2018**, *27*, 075007.
[16] Y. Pei, H. Zhong, M. Wang, P. Zhang, Y. Zhao, *Nanomaterials* **2018**, *8*, 732.
[17] Y. Hayamizu, T. Yamada, K. Mizuno, R. C. Davis, D. N. Futaba, M. Yumura, K. Hata, *Nat. Nanotechnol.* **2008**, *3*, 289.
[18] T. Yamada, N. Makiomoto, A. Sekiguchi, Y. Yamamoto, K. Kobashi, Y. Hayamizu, Y. Yomogida, H. Tanaka, H. Shima, H. Akinaga, D. N. Futaba, K. Hata, *Nano Lett.* **2012**, *12*, 4540.
[19] P. P. Abadi, M. R. Maschmann, J. W. Baur, S. Graham, B. A. Cola, *Nanotechnology* **2013**, *24*, 475707.
[20] R. H. Poelma, X. Fan, Z.-Y. Hu, G. Van Tendeloo, H. W. van Zeijl, G. Q. Zhang, *Adv. Funct. Mater.* **2016**, *26*, 1233.

[21] Y. Cai, S. R. Shah, A. Zimmermann, M. Weinmann, R. Raj, F. Aldinger, *Phys. Status Solidi A* **2002**, *193*, R13.
[22] B. L. Smith, T. E. Schäffer, M. Viani, J. B. Thompson, N. A. Frederick, J. Kindt, P. K. Hansma, *Nature* **1999**, *399*, 761.
[23] J. B. Thompson, J. H. Kindt, B. Drake, H. G. Hansma, D. E. Morse, P. K. Hansma, *Nature* **2001**, *414*, 773.
[24] D. Qian, W. Liu, R. S. Ruoff, *Compos. Sci. Technol.* **2003**, *63*, 1561.
[25] R. B. Pipes, P. Hubert, J.-P. Salvetat, L. Zalamea, *Compos. Sci. Technol.* **2006**, *66*, 1125.
[26] R. B. Pipes, L. Zalamea, *Compos. Sci. Technol.* **2006**, *66*, 2844.
[27] K. T. Kashyap, R. G. Patil, *Bull. Mater. Sci.* **2008**, *31*, 185–187.
[28] A. N. Sohi, P. M. Nieva, *J. Micromech. Microeng.* **2014**, *24*, 115004.
[29] J. Lai, T. Perazzo, Z. Shi, A. Majumdar, *Sens. Actuators A* **1997**, *58*, 113.
[30] Y. Zhao, M. Mao, R. Horowitz, A. Majumdar, J. Varesi, P. Norton, J. Kitching, *J. Microelectromech. Syst.* **2002**, *11*, 136.
[31] J. R. Barnes, R. J. Stephenson, C. N. Woodburn, S. J. O'Shea, M. E. Welland, T. Rayment, J. K. Gimzewski, C. Gerber, *Rev. Sci. Instrum.* **1994**, *65*, 3793.

Manuscript received: January 8, 2020
Accepted manuscript online: January 31, 2020
Version of record online: February 19, 2020